scientific reports

Check for updates

OPEN

A versatile gold leaf immunosensor with a novel surface functionalization strategy based on protein L and trastuzumab for HER2 detection

Ivana Kundacina[1]✉, Silvia Schobesberger[2], Stefan Kittler[3], Helena Thumfart[2], Oliver Spadiut[3], Peter Ertl[2], Nikola Ž. Knežević[1] & Vasa Radonic[1]✉

Although various sensors specifically developed for target analytes are available, affordable biosensing solutions with broad applicability are limited. In this study, a cost-effective biosensor for detecting human epidermal growth factor receptor 2 (HER2) was developed using custom-made gold leaf electrodes (GLEs). A novel strategy for antibody immobilization on a gold surface, for the first time mediated by protein L and HER2-specific antibody trastuzumab, was examined using commercial screen-printed gold electrodes and GLEs. A self-assembled monolayer of 11-mercaptoundecanoic acid (MUA) was formed on the gold surface, which was used to covalently immobilize protein L. Further binding of trastuzumab to the protein L was employed and HER2 detection was achieved through electrochemical impedance spectroscopy (EIS). The HER2 detection was examined in phosphate-buffered saline (PBS) and supplemented cell culture medium. The modified GLEs showed good specificity and high sensitivity of HER2 detection without any enrichment steps, achieving a limit of detection (LOD) of 1 ng mL^{-1} in PBS and 2.7 ng mL^{-1} in cell culture medium, making the proposed immunosensor a cost-effective and sensitive solution for detection in complex biological matrices.

Keywords Gold leaf electrodes, Cancer biomarker detection, Electrochemical immunosensor, Protein L, Trastuzumab, HER2 biosensor

Breast cancer is one of the most commonly diagnosed types of cancer in women worldwide. According to the World Health Organization (WHO), 2.3 million women were diagnosed with breast cancer in 2020, resulting in 685,000 deaths[1], while the survival rate for metastatic cancer is only 20% at 5 years[2]. For that reason, timely detection of specific cancer biomarkers, such as human epidermal growth factor receptor 2 (HER2), is crucial in battling this disease. HER2 is a protein receptor that plays a key role in the regulation of cell growth and division. In healthy individuals, the presence of HER2 is essential for maintaining healthy tissue, but mutations that lead to overexpression of HER2 are associated with aggressive forms of breast cancer. In the blood of healthy people, the concentration of HER2 is in the range of 4–14 ng mL^{-1}, while in HER2-positive breast cancer patients, the level increases to 15–75 ng mL^{-1}[3,4]. In general, HER2-positive patients have a more aggressive form of the disease and a worse prognosis than HER2-negative patients. Notably, in 1998 and 2000 in the USA and European Union, respectively, Herceptin (trastuzumab) was approved for medical applications for the treatment of HER2-positive breast cancer patients[5]. This monoclonal antibody acts by targeting and blocking HER2 on the surface of cancer cells from receiving growth signals.

Standard methods for breast cancer diagnostics include techniques based on imaging like ultrasound, magnetic resonance, and molecular breast imaging; gene expression techniques such as radioimmunoassay, immunohistochemistry, and enzyme immunoassay; and invasive methods such as biopsy[6]. However, novel solutions for cancer biomarker detection are based on the development of biosensors and their integration into point-of-care devices for routine blood testing.

[1]University of Novi Sad, BioSense Institute, Dr Zorana Djindjica 1, Novi Sad 21000, Serbia. [2]Faculty of Technical Chemistry, TU Wien, Getreidemarkt 9, Vienna 1060, Austria. [3]Research Division Integrated Bioprocess Development, Institute of Chemical, Environmental and Bioscience Engineering, TU Wien, Gumpendorfer Strasse 1a, Vienna 1060, Austria. ✉email: ivana.kundacina@biosense.rs; vasarad@biosense.rs

Different optical[7,8], field effect transistor-based[9,10], colorimetric[11–13], mass-change[14,15], and electrochemical biosensors[16–18] have been proposed for early-stage diagnostics of breast cancer[19]. Among the proposed solutions, electrochemical biosensors have shown the potential to achieve the best sensitivity by introducing low-cost materials[20–23], nanomaterials[24,25], examining different immobilization protocols of biorecognition elements[26–28], and signal amplification strategies[29]. Gold electrodes are widely used substrates for biosensing applications due to their excellent electrical conductivity and chemical inertness which provide stable and reliable measurements. Additionally, gold surfaces facilitate easy functionalization through self-assembled monolayers of thiol-containing molecules, enabling effective immobilization of biorecognition elements. Even though the production of low-cost gold electrodes is challenging[22,23], we recently reported a novel technology that allows the construction of multiple electrodes in a single batch, with enhanced surface roughness for sensitive detection of bacteria *Escherichia coli* (*E. coli*) and *Salmonella Typhimurium* without any enrichment steps[30,31].

In addition to the gold surface and structural quality, devising the appropriate sensing layer and immobilized biorecognition elements is an important step in biosensor development. Protein L is a versatile binding ligand with unique capabilities for the detection and purification of antibodies and antibody fragments. Unlike other affinity ligands such as protein A or G, protein L interacts with immunoglobulin light chains. Despite the potential of protein L as a binding ligand and antibody purification in previous studies[32–34], no electrochemical biosensor incorporation of this ligand has been employed so far. Protein L exhibits remarkable specificity for the detection of antibody fragments and monoclonal antibodies, especially IgGs derived from humans[32,35,36], , making it a good candidate as a versatile biosensing platform for antibody immobilization.

For such purpose, we set forth to develop a gold leaf electrode (GLE)-based electrochemical biosensor for the detection of the cancer biomarker HER2, mediated by surface-functionalized protein L and its capabilities to further bind the HER2-targeting monoclonal antibody trastuzumab. The biosensor design was guided by the goal of achieving a response resembling a typical Randles equivalent circuit, and realization of a low-cost and rapid testing prototype. The produced GLEs were characterized in terms of composition, electroactive surface, and responsiveness to different concentrations of redox probes prepared in deionized water (DIW), potassium chloride, and phosphate-buffered saline (PBS). In addition, the antibody immobilization was examined and characterized via a fluorescence immunoassay, bio-layer interferometry, and electrochemical impedance spectroscopy (EIS). The detection sensitivity was electrochemically tested using commercial gold screen-printed electrodes and GLEs. Finally, the application potential of the GLE-based biosensor was validated for the detection of HER2 in the cell culture medium.

Materials and methods

Materials and fabrication of gold leaf electrodes

As it was described in our previous work[30], two layers of gold leaves (Pozlata Dimitrijevic, Serbia) were laminated at 180 °C (Laminator PDA3 330 C, PINGDA, China) on the surface of 0.5 mm thick multilayered structure of PVC sheets (Fellowes Brands, Poland) covered with polytetrafluoroethylene – PTFE spray (Wurth, Serbia). The laser ablation of a gold leaf sheet was performed using a Nd: YAG laser (Power Line D-100, Rofin-Sinar, Germany) in order to realize the electrode geometry.

Chemicals

Sulfuric acid (H_2SO_4), Dulbecco's PBS (modified without $CaCl_2$ and $MgCl_2$), 11-mercaptoundecanoic acid (MUA), N-hydroxysuccinimide (NHS), bovine serum albumin (BSA), Tween® 20, potassium chloride (KCl), sodium carbonate (Na_2CO_3), sodium bicarbonate ($NaHCO_3$), potassium ferricyanide ($K_3[Fe(CN)_6]$), and potassium ferrocyanide ($K_4[Fe(CN)_6]\cdot 3H_2O$) were purchased from Sigma-Aldrich (USA), while 1-Ethyl-3-(3-dimethylaminopropyl)carbodiimide hydrochlorid (EDC-HCl), Peptipure ≥ 99% were procured from ROTH and absolute ethanol from Chem-Lab NV (Belgium). Human HER2 was purchased from ACRO Biosystems (USA), antibody for *E. coli* (ab137967) from Abcam (USA), and Fibrinogen (FBG) from CSL Behring (USA). Fluorescent probe Alexa Fluor 488, anti-human IgG (H + L) (Invitrogen), and Cell culture medium (Gibco CO_2 Independent Medium) were purchased from Thermo Fisher Scientific. Cell culture medium supplemented with 10% serum (Fetal Bovine Serum, Sigma-Aldrich), 1% antibiotics (Penicillin-Streptomycin, Sigma-Aldrich), and 1% L-glutamine. Protein L was recombinantly produced in *E. coli* and characterized as described in[36].

Equipment

Electrochemical measurements were performed using the Multichannel Potentiostat (Biologic VMP-3e, France) connected to a PC with EC-lab software. Fluorescence measurements were done using a Multimode plate reader (EnSpire® 2300, Perkin Elmer), and bio-layer interferometry using an Octet RED96e (PALL FortéBio, CA, USA) device. A connection of electrodes (custom-made GLEs and commercial screen-printed electrodes, Dropsens 220AT, Metrohm) with the potentiostat was realized using a holder (Original 1 PCS 2.54 mm Single Row 3P PCB Clip Clamp Fixture Probe Pogo Pin, China).

Bio-layer interferometry

The functionality of protein L was verified with bio-layer interferometry. Namely, different concentrations of protein L (0.002, 0.004, 0.006, 0.008, 0.015, and 0.03 mg/mL, respectively) were incubated with trastuzumab and their binding with trastuzumab was examined.

Functionalization steps

For the functionalization of the biosensor, 1 mM MUA prepared in absolute ethanol was incubated at the working electrode (WE) at 4 °C. The concentration of 1 mM was chosen between examined 1 mM, 5 mM, and 10 mM in order to realize half-circle and a diffusion tail in Nyquist plot, which is described with Randles

circuit, Fig. S.4. The droplet of 1 mM MUA with a volume of 1 µL was drop cast on the WE, and the incubation was done in the dark. After 16 h of incubation, rinsing of the electrode surface was done initially with absolute ethanol, and then with DIW. Activation of carboxyl groups of MUA was performed by applying 10 µL of 50 mM NHS/50 mM EDC prepared in PBS, to the WE by one-hour incubation in the dark. The electrode was then rinsed with DIW. Activated carboxyl groups have an affinity for binding amino groups of proteins, so in the next step of functionalization, 10 µL of protein L with 0.1 mg mL^{-1} concentration was incubated for 1 h. After incubation and rinsing protein L, a BSA concentration of 50 µg mL^{-1} was applied and incubated for 20 min in the dark to prevent a non-specific binding or non-specific contribution to the signal. Subsequently, trastuzumab with concentrations in the range of 0.1 ng mL^{-1} to 1000 ng mL^{-1} was incubated for 20 min, rinsed with DIW, and characterized with the redox probe in EIS measurements. After exposing the electrode to an increasing concentration of trastuzumab, the electrode was exposed to increasing concentrations of HER2 in the range of 0.1 ng mL^{-1} to 1000 ng mL^{-1}. The incubation of 20 min, rinsing with DIW, and EIS characterization were repeated for each concentration of HER2. Finally, the robustness of the biosensor and the detection method was tested in a cell culture medium (10% serum, 1% antibiotics, 1% L-glutamine, and 88% medium). HER2 in the range of 0.1 ng mL^{-1} to 1000 ng mL^{-1} was measured in a 10-fold diluted cell culture medium.

Electrochemical characterization of gold leaf electrodes

The CV characterization of bare GLE in 0.5 M sulphuric acid was obtained in the potential range from 0 V to 1.55 V vs. gold reference electrode (RE) and scan rate 0.5 V s^{-1}, while stability tests were performed with the redox probe in the potential range from −0.4 V to 0.4 V vs. gold RE. The scan rate was 0.5 V s^{-1} and a voltammogram was made in 100 cycles. In addition, the electroactive surface was determined from the series of experiments with the redox probe in the same potential range, for cycles made with scan rates in the range of 0.1 V s^{-1}– 1 V s^{-1} with steps of 0.1 V s^{-1}. The linear dependence of the square root of the scan rate and oxidation and reduction peaks were used to calculate the electroactive surface of the electrodes from the slope using the Randles-Sevcik equation[37] given by (1):

$$A = \frac{k}{2.69 \cdot 10^5 \cdot C \cdot D^{1/2} \cdot n^{3/2}} \quad (1)$$

where k represents the slope coefficient of the linear dependence, $2.69 \cdot 10^5$ C mol^{-1} $V^{-1/2}$ constant, C concentration of ions, n the number of electrons participating in the half-reaction, and D the diffusion coefficient ($6.1 \cdot 10^{-6}$ cm^2 s^{-1})[38].

The biosensor detection of HER2 was based on the EIS principle. EIS measurements were done in the frequency range of 1 Hz to 100 kHz, with a direct potential set to zero and a potential amplitude of 10 mV. All measurements were performed versus an open circuit potential in a two-electrode system, where counter and reference electrodes were connected to the same potential.

Fluorescence immunoassay

The fluorescent assay was done in a 96-well plate, and measurements were performed with a plate reader. Initially, the wells were coated with 0.5 µg mL^{-1} protein L or 0.5 µg mL^{-1} HER2 and incubated overnight at 4 °C. Then the plate was washed 4 times with 200 µL of washing buffer (PBS + 0.05% Tween20). Afterward, 100 µL of trastuzumab was added and incubated for 2 h at room temperature. The washing procedure was repeated 4 times with 200 µL of washing buffer and subsequently, a secondary antibody with a fluorescent probe was added in the next step. Briefly, 100 µL of 1:1000 diluted fluorescent goat anti-human IgG was added to the plate wells and incubated for 1 h at room temperature. Afterward, the plate was rinsed 6 times with 200 µL of washing buffer and fluorescence was measured.

Matrix effect and recovery test

Matrix effect and recovery tests were conducted to evaluate the biosensor's performance in the complex matrix, i.e. diluted cell culture medium. The matrix effect was assessed by comparing the biosensor's response to the HER2 biomarker in PBS and spiked cell culture medium, with the matrix effect percentage calculated as the ratio of the signal in the matrix to the signal in PBS. Recovery was determined by spiking known concentrations of HER2 into the cell culture medium, measuring the biosensor's response, and calculating the percentage of the detected concentration relative to the spiked amount.

Results

Electrode configuration

Figure 1a presents a planar three-electrode system design, where the WE, counter, and reference electrodes were realized in gold leaves. The overall dimension of the platform is 10.7 × 28.7 mm, with a pin distance of 2.54 mm which corresponds to standard electronic connecting components. In order to compare the responses of GLEs with commercial screen-printed electrodes, the WE radius was set to 2 mm, which is the same as the radius of commercial electrodes.

Biosensor development

A schematic view of the functionalization layers is presented in Fig. 1b. A self-assembled monolayer of MUA is formed by the binding of thiol groups to the gold surface. The carboxyl group on the opposite end provides MUA with the possibility of binding protein L, by activating the carboxyl groups using NHS/EDC chemistry. The affinity of protein L for binding IgG antibodies enables trastuzumab immobilization and subsequently detection of HER2 cancer biomarker. To prevent non-specific binding, BSA is introduced as a blocking step

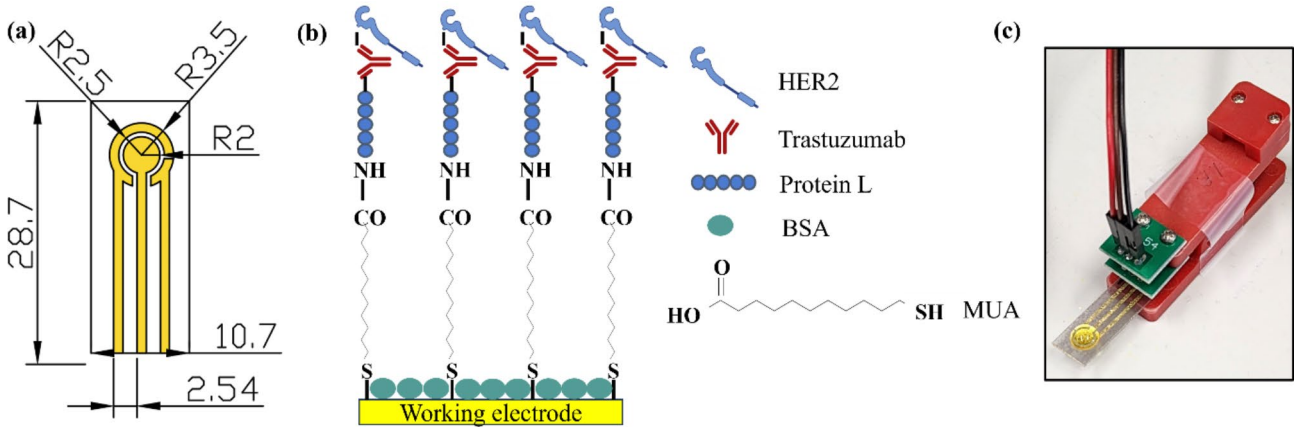

Fig. 1. (**a**) Dimensions of the GLE in mm, R = radius; (**b**) Biosensor functionalization; (**c**) Experimental setup.

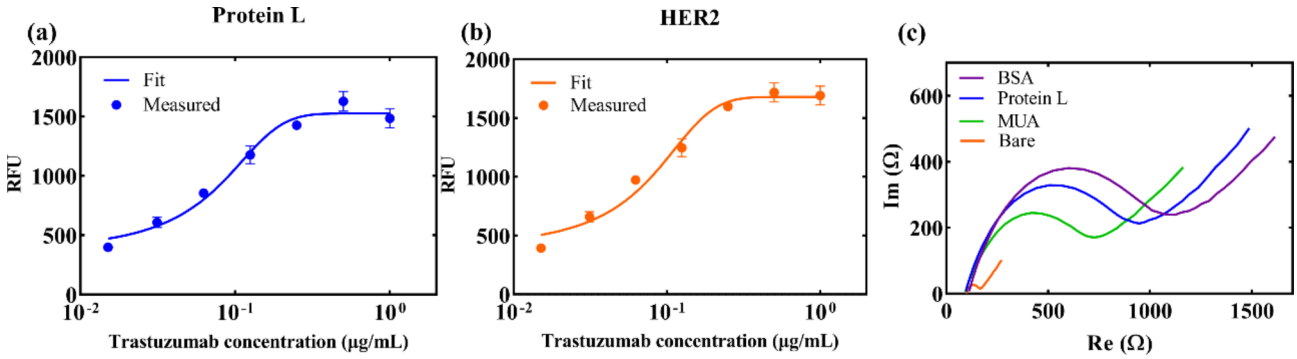

Fig. 2. (**a**) Fluorescence immunoassay, binding of trastuzumab with protein L; Error bars present standard deviation of three samples; (**b**) Fluorescence immunoassay, binding of trastuzumab with HER2; Error bars present standard deviation of three samples; (**c**) Electrochemical characterization of each functionalization step on GLE.

in the functionalization process. The experimental setup is shown in Fig. 1c, where the GLE is placed in the electrode holder with 60 µL droplet volume.

Electrochemical characterization of GLEs

The described GLEs were characterized in terms of composition, effective surface area, and signal stability through CV experiments. In addition, the response of EIS was used to examine the sensitivity for different concentrations of potassium ferro/ferricyanide redox probes prepared in DIW, potassium chloride, and PBS. Full electrochemical characterization of GLE and its roughness in comparison to the commercial Dropsens electrodes is available in the Supplemental information (Figs. S.1 - S.3).

Fluorescence immunoassay and Bio-layer Interferometry

As previously mentioned, a fluorescence immunoassay was used to confirm the binding of protein L and trastuzumab, as well as trastuzumab and HER2 in the range of 0.015 µg mL^{-1} to 1 µg mL^{-1}, as shown in Fig. 2a and b. Both results show binding events, i.e., the signal increases with higher trastuzumab concentrations. An S-curve was used for data fitting, showing a linear trend in the concentration range 0.03 µg mL^{-1} to 0.25 µg mL^{-1}, after which a saturation can be observed both for protein L and HER2. Besides, the results of bio-layer interferometry demonstrate a concentration-dependent binding signal between protein L and trastuzumab. This further validates the effective interaction between protein L and trastuzumab, confirming its suitability for antibody immobilization in biosensing applications. (Fig. S.5).

Electrochemical characterization of functionalization steps

The binding of each functionalization layer to the WE was characterized electrochemically by EIS. Figure 2c presents Nyquist plots after each functionalization step for GLE, while for the Dropsens electrode, the plot is shown in Fig. S.6. Clearly, after each functionalization step (MUA, protein L, BSA) impedance increases due to the increased coverage of the Au surface with dielectric molecules.

To further characterize the functionalized surface, increasing concentrations of trastuzumab in the range of 0.1 ng mL^{-1} to 1000 ng mL^{-1} were incubated with the protein L-functionalized electrodes, and the results

of EIS readouts are shown in Fig. 3a (for Dropsens electrode Fig. S.7). With higher trastuzumab concentration, the number of antibodies bound to protein L on the electrode surface increases, which is reflected in the rise of impedance.

Detection of HER2 with Dropsens and GLEs in PBS

After repeated incubations with trastuzumab, the final structure of the biosensor was exposed to increasing concentrations of the cancer biomarker HER2 in the range of 0.1 ng mL^{-1} to 1000 ng mL^{-1}. The results in Fig. 3b clearly show an increase in impedance with elevated HER2 concentration, which is in accordance with the expected rise in impedance upon binding the HER2 to the surface. Finally, the results were fitted with a standard Randles circuit[39] (where R_{sol} presents solution resistance, R_{ct} charge transfer resistance, W Warburg element, and CPE constant phase element) presented in insets of Fig. 3c and d. The relative signal change was calculated in relation to the BSA-functionalized electrode for results of trastuzumab binding, while for HER2 detection, it was in relation to the signal obtained for the presence of trastuzumab at a concentration of 1000 ng mL^{-1}. For GLEs, the results in Fig. 3c show an increase in the relative change with the elevating concentration of trastuzumab, while in the case of the Dropsens electrode saturation of the signal is evidenced beyond the concentration of 100 ng mL^{-1}. The detection response of trastuzumab for GLE is described by a linear equation $y = 39.978x + 62.195$, $R^2 = 0.9854$, (Dropsens electrode: $y = 14.118x + 17.774$, $R^2 = 0.9763$). Both electrodes demonstrated a good linearity in detecting trastuzumab using the proposed configuration. For the detection of the cancer biomarker, as shown in Fig. 3d, the GLE exhibited a linear growing trend in the range of 0.1–1000 ng/mL, described by the equation $y = 12.145x + 24.589$, $R^2 = 0.9507$, while the Dropsens HER2 detection curve showed a typical sigmoid shape with saturation after 10 ng mL^{-1}. Thus, in the case of the prepared biosensors for HER2, the GLE-based

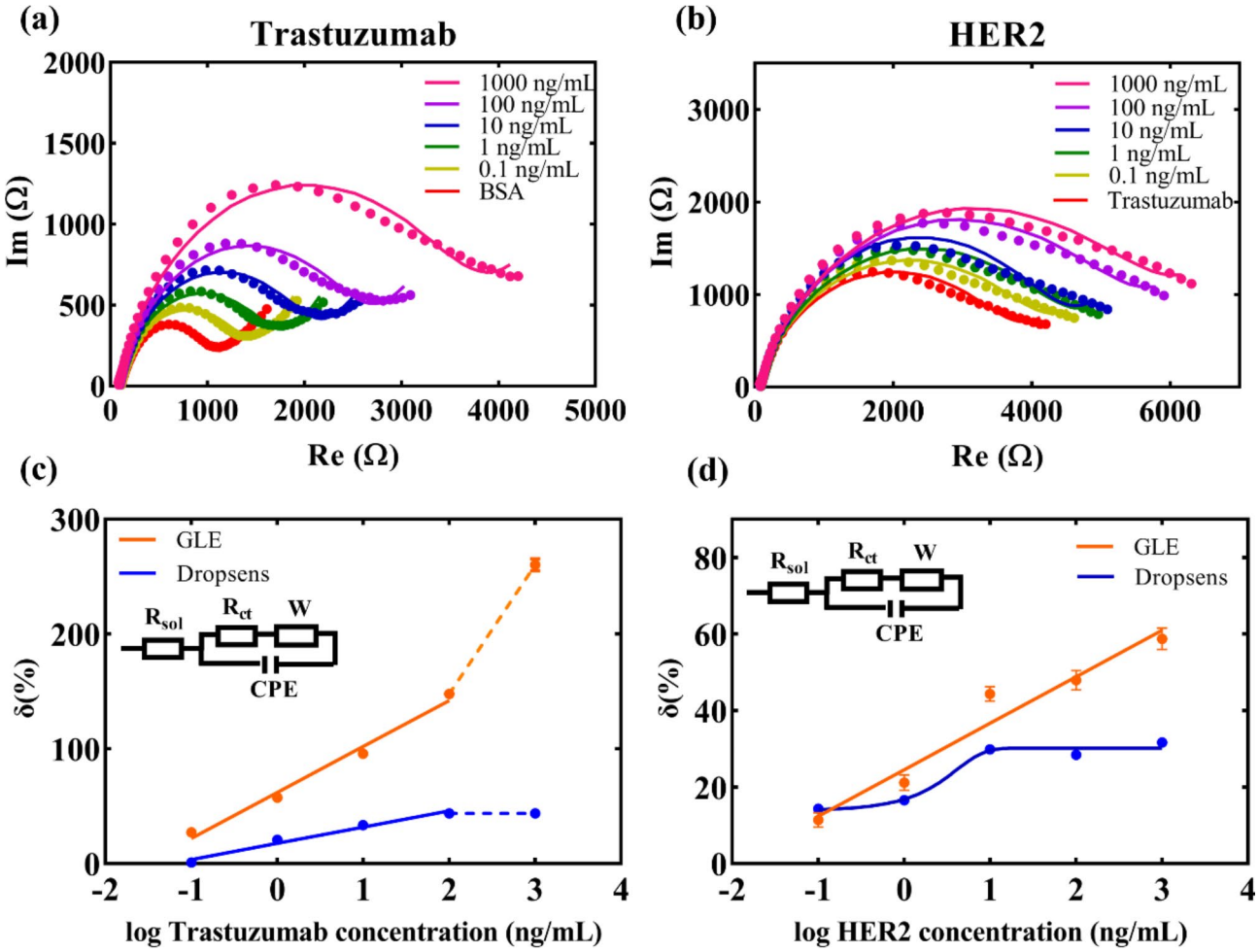

Fig. 3. (**a**) Nyquist plots for different concentrations of trastuzumab; (**b**) Nyquist plots for different concentrations of HER2; (**c**) Comparison of the relative change of the signal versus BSA saturated electrode for different concentrations of trastuzumab – GLE and Dropsens responses; Results are presented as mean value of three measurements with standard deviation. (**d**) Comparison of the relative change of the signal versus trastuzumab saturated electrode for different concentrations of HER2 – GLE and Dropsens responses. Results are presented as a mean value of three measurements with standard deviation. The presented results demonstrate significantly better performance in sensor detection realized using GLEs compared to Dropsens electrodes.

detection shows promising results for a wide range of HER2 concentrations, while the Dropsens-based detection would not be suitable as the saturation of the signal is achieved at a lower concentration than in the case of HER2 positive cancer patients.

Specificity tests

To test the specificity of the developed biosensor, the detection was examined with non-specific proteins prepared in PBS. Figure 4a presents the compared detection responses for different concentrations of the specific biomarker HER2 and non-specific proteins such as *E. coli* antibody, BSA, and fibrinogen (FBG) prepared in PBS, tested at a concentration of 100 ng mL^{-1}. The presented results show that the signals of the specific biomarker for concentrations > 1 ng mL^{-1} are significantly higher compared to non-specific ones. In real samples, large concentrations of non-specific proteins are rarely found, so this result does not diminish the detection potential of the proposed sensor.

Detection of HER2 in cell culture medium

Considering that the medium is a complex matrix with numerous non-specific components that may contribute to the signal and lead to higher impedance, a control involving surface saturation of the electrode by incubating the medium without the specific biomarker was conducted. Initially, the sensor saturation was performed during a 2-hour incubation of the medium without the cancer biomarker. Subsequently, a repeated incubation of the medium for 20 min was done to confirm the signal's constancy without the cancer biomarker. This step aimed to determine whether the signal contribution originated from the specific biomarker rather than non-specific components of the medium, which might adhere to the surface due to electrostatic or other interactions. The

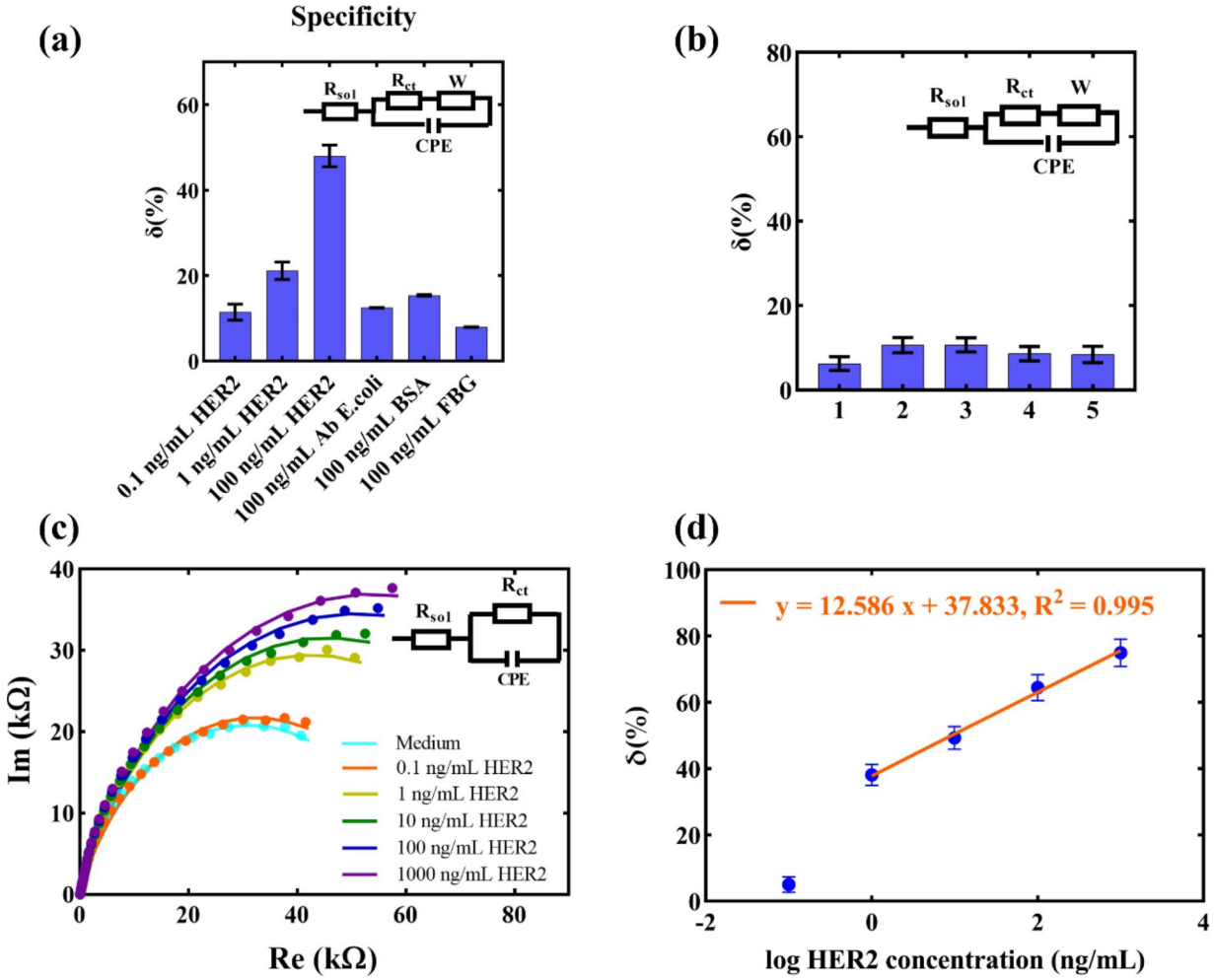

Fig. 4. (**a**) Specificity tests for GLE-based HER2 immunosensor (AB = antibody, FBG = fibrinogen); Results are presented as mean value with standard deviation ($n = 3$). (**b**) Control test: Repeated cell culture medium incubation after surface saturation; Results are presented as mean value with standard deviation ($n = 3$). (**c**) Nyquist plots with an equivalent Randles circuit used for fitting the data of HER2 detection in cell culture medium; (**d**) Relative change of the signal versus medium saturated surface for different concentrations in the cell culture medium. Error bars in the graph present standard deviations of three measurements.

Spiked concentration (ng/mL)	Response in buffer (%)	Response in medium (%)	Matrix effect (%)
0.1	12.4	25.2	202.9
1	24.6	37.8	153.9
10	36.7	50.4	137.3
100	48.9	63.0	128.9
1000	61.0	75.6	123.9

Table 1. Matrix effect analysis.

Spiked concentration (ng/mL)	Measured concentration (ng/mL)	Recovery (%)
1	1.1	105.2
10	8.1	80.9
100	131.4	131.4
1000	894.8	89.5

Table 2. Recovery analysis.

results in Fig. 4b show a consistent signal after the repeated incubation of the medium, confirming that the electrode is saturated with non-specific components from the medium. This control ensures that any contribution to the increase in impedance in samples with HER2 would not originate from the medium.

Final validation for the detection of the cancer biomarker in the medium was conducted by incubating the electrode for 20 min with increasing concentrations of the cancer biomarker in a cell culture medium, using a GLE previously saturated with the medium. The graph in Fig. 4c shows sensor response results with Nyquist plots without a diffusion tail. For this reason, the proposed electrical circuit for fitting the results, presented in the inset graph, does not include a Warburg element. Additionally, the results show that the impedance increases linearly with higher HER2 concentrations. The curve representing the dependence of the relative change in charge transfer resistance is shown in Fig. 4d, for HER2 concentrations in the range 1–1000 ng/mL, showing a linear relationship described by the equation $y = 12.586x + 37.833$, $R^2 = 0.995$. These presented results demonstrate the excellent detection potential of the proposed biosensor, even in complex matrices such as cell culture medium.

Matrix effect and recovery test

The matrix effect analysis, presented in Table 1, demonstrated that the biosensor's response in the cell culture medium was consistently higher than in the buffer across all concentrations, with matrix effect values ranging from 123.9 to 153.9%. At the lowest concentration of 0.1 ng/mL, the matrix effect was the highest at 202.9%, likely due to significant noise originating from the complex cell culture medium, which disproportionately affected the signal. This resulted also in increasing the limit of detection (LOD) above the lowest tested concentration (0.1 ng/mL), which was therefore outside of the linear range of the detection in medium. Recovery values are given in Table 2 and range from 80.9 to 131.4%.

Discussion

In this study, protein L was used for the immobilization of antibodies on the electrode surface for application in electrochemical biosensing for the first time. In contrast, proteins A and G, well-known immunoglobulin binding proteins, were already proposed in the literature for the immobilization and functionalization of biosensors[35]. These proteins are commonly used in antibody purification, either covalently attached to agarose or as bioconjugated nanoparticles[35,40]. Protein L possesses a distinctive advantage attributable to its specific interaction with kappa light chains, facilitating the binding to a broader range of immunoglobulins, including antibody fragments as well[32]. Consequently, we believe the proposed strategy of immobilizing antibodies and fragments through protein L is a promising strategy to establish a universal platform, circumventing the necessity for the individual development of biosensors at the initial stage of immobilization.

The potential of the proposed immunosensor was validated by binding anticancer monoclonal antibody trastuzumab to protein L-functionalized surface and detecting the HER2 biomarker in PBS and a diluted supplemented cell culture medium. The limit of detection (LOD) was calculated by Eq. $3\sigma/S$ where σ is the standard deviation of a blank test and S is the slope of the calibration curve[41]. Detection limits were determined to be 1 ng mL^{-1} in PBS, and 2.7 ng mL^{-1} in cell culture medium. The immunosensor showed higher LOD in the complex matrix since the sensing surface was saturated with non-specific components of the cell culturing medium and probably partially blocked the specific binding places on the biosensor surface. Matrix effect analysis revealed a moderate impact on the biosensor's performance at higher concentrations, with matrix effect values ranging from 123.9 to 153.9%, while at the lowest concentration of 0.1 ng mL^{-1}, a pronounced matrix effect of 202.9% was observed due to significant noise in the complex medium. Recovery values, on the other hand, fell within acceptable boundaries across most tested concentrations, with recovery rates ranging from 80.9 to 131.4%. These results confirm the biosensor's ability to provide reliable detection in complex matrices, although with slight variability at lower concentrations due to matrix interactions. Nevertheless, these values

Detection method	Material	Biorecognition element	Dynamic range (ng mL^{-1})	LOD (ng mL^{-1})	Ref.
DPV[4]	Graphene-decorated rhodium nanoparticles	Aptamer	10–500	0.667	[4]
DPV	GCE with PEDOT and peptide hydrogel	Antibody	0.1–1000	45×10^{-3}	[43]
DPV	GCE with PEG and AuNPs	Peptide	0.001–1000	4.4×10^{-4}	[44]
DPV	GCE with antiHER2/APTMS[1]-Fe_3O_4	Antibody	$5\times10^{-4}-50$	2×10^{-5}	[45]
DPV	SP gold electrode	Antibody	0.5–25	0.59	[42]
DPV	AuNPs@HRP[2]@ZIF-8	Peptide	$50\times10^{-6}-50$	16.8×10^{-6}	[46]
SQV[5]	Cd^{2+}- aptamer@AMNFs@ZIF-67 nanocomposite	Aptamer	0–1000	4.8×10^{-6}	[47]
SQV	GCE with PEDOT: PSS[3] and AuNPs	Aptamers	0.01–1000	1.979×10^{-6}	[48]
EIS	Gold leaf electrodes	Antibody	1–1000	1	This work

Table 3. Comparison of the proposed sensor with other biosensors from the literature. [1]3-aminopropyltrimethoxysilane, [2]horseradish peroxidase, [3]poly (3,4-ethylenedioxythiophene): polystyrene sulfonate, [4]differential pulse voltammetry, [5]square wave voltammetry.

are lower than the concentrations of HER2 detectable in healthy individuals and HER2-positive patients, making the proposed immunosensor a good candidate for cancer biomarker sensing. Besides sensing HER2, we demonstrated the potential of the proposed immunosensor to detect the antibody (trastuzumab), which is also being employed for cancer therapy. Even though the sensing of trastuzumab would not be specific, due to the robust abilities of protein L for binding antibodies, this highlights the broad capabilities of the protein L-mediated approach for construction of biosensors with potential sensing applications in the pharmaceutical industry to monitor antibody (fragment) expression, purification and quality control.

Table 3 compares the GLE-based HER2 biosensor with other electrochemical biosensors proposed in the literature. In general, commonly used substrates for electrochemical detection are gold[42] and carbon electrodes[43]. To increase the effective surface area, amplify the signal and immobilize biorecognition elements for the sensor surface, nanomaterials of different dimensionalities were used: nanoparticles such as gold[44–46], rhodium[4], and iron[45], 2D nanomaterials like antimonene (AMNFs)[47], graphene and graphene oxide[4] and 1D nanomaterials like carbon nanotubes[48]. Recent studies incorporated metal-organic frameworks (MOFs) for biosensor implementation with exceptionally sensitive detection properties[46,47] with LODs in femtograms per milliliter. Other studies use conductive polymers and hydrogels[43,44] for the detection of biomarkers. Each of the proposed biosensors, with its LOD and dynamic detection range, meets the requirements for the sensitivity and specificity of HER2 cancer biomarker detection. However, the proposed technologies require a facility for nanotechnology, expensive equipment, chemicals, and trained personnel for the realization of each described sensor. Furthermore, the proposed method based on GLEs exceeds all other solutions in terms of simplicity and price of substrate fabrication. Multiple electrodes can be produced from a single batch, reducing the estimated cost of each electrode to one-tenth of that of commercial screen-printed electrodes. Additionally, the production of protein L was optimized previously, reducing the price of this affinity ligand significantly[36].

Conclusions

In this study, a cost-effective immunosensor for the detection of trastuzumab and the cancer biomarker HER2 using custom-made GLEs was presented. The biosensor employed a novel strategy for immobilization of HER2-targeting antibody trastuzumab on a gold surface mediated by protein L. The modified GLEs exhibited a high specificity and sensitivity for HER2 detection without requiring enrichment steps. The proposed immunosensor achieved LOD of 1 ng mL^{-1} in PBS and 2.7 ng mL^{-1} in cell culture medium, which meets the requirements for the detection of HER2. In addition, the biosensing principle employing protein L as an immobilization element may open the possibilities for adapting the biosensor to bind different types of antibodies with different analyte binding capabilities. The presented results highlight the excellent characteristics of GLEs and the employed surface functionalization for efficient HER2 detection. This advancement opens the possibility for the future development of affordable, point-of-care biosensing devices, which could revolutionize the detection and monitoring of HER2-positive breast cancer patients. By enabling rapid, accurate, and accessible diagnostics, such devices have the potential to greatly improve patient care and treatment outcomes.

Data availability

All data generated or analyzed during this study are included in this published article (and its supplementary information files).

Received: 13 September 2024; Accepted: 18 December 2024
Published online: 02 January 2025

References

1. World Health Organisation. Breast cancer statistics. https://www.who.int/news-room/fact-sheets/detail/breast-cancer (2023).
2. Boix-Montesinos, P., Soriano-Teruel, P. M., Armiñán, A., Orzáez, M. & Vicent, M. J. The past, present, and future of breast cancer models for nanomedicine development. *Adv. Drug Deliv Rev.* **173**, 306–330 (2021).
3. Arya, S. K. et al. Capacitive aptasensor based on interdigitated electrode for breast cancer detection in undiluted human serum. *Biosens. Bioelectron.* **102**, 106–112 (2018).

4. Sadeghi, M., Kashanian, S., Naghib, S. M. & Arkan, E. A high-performance electrochemical aptasensor based on graphene-decorated rhodium nanoparticles to detect HER2-ECD oncomarker in liquid biopsy. *Sci. Rep.* **12**, 3299 (2022).
5. Lebeau, A. Herceptin therapy in breast cancer: new indication? *Verh Dtsch. Ges Pathol.* **90**, 99–106 (2006).
6. Chupradit, S. et al. Recent advances in biosensor devices for HER-2 cancer biomarker detection. *Anal. Methods*. **14**, 1301–1310 (2022).
7. Akgönüllü, S. & Denizli, A. Recent advances in optical biosensing approaches for biomarkers detection. *Biosens. Bioelectron. X*. **12**, 100269 (2022).
8. Nejati-Koshki, K., Fathi, F., Arabzadeh, A. & Mohammadzadeh, A. Biomarkers and optical based biosensors in cardiac disease detection: early and accurate diagnosis. *Anal. Methods*. **15**, 5441–5458 (2023).
9. Hao, R., Liu, L., Yuan, J., Wu, L. & Lei, S. Recent advances in field effect transistor biosensors: designing strategies and applications for sensitive assay. *Biosensors* **13**, (2023).
10. Li, L. et al. Carbon nanotube field-effect transistor biosensor with an enlarged gate area for ultra-sensitive detection of a lung cancer biomarker. *ACS Appl. Mater. Interfaces*. **15**, 27299–27306 (2023).
11. Chi, Y. J., Ryu, B., Ahn, S. & Koh, W. G. A colorimetric biosensor based on a biodegradable fluidic device capable of efficient saliva sampling and salivary biomarker detection. *Sens. Actuat B-Chem*. **396**, 134601 (2023).
12. Hasan, M. R., Sharma, P., Pilloton, R., Khanuja, M. & Narang, J. Colorimetric biosensor for the naked-eye detection of ovarian cancer biomarker PDGF using citrate modified gold nanoparticles. *Biosens. Bioelectron. X*. **11**, 100142 (2022).
13. Xiao, L. et al. Colorimetric biosensor for detection of cancer biomarker by au nanoparticle-decorated Bi2Se3 nanosheets. *ACS Appl. Mater. Interfaces*. **9**, 6931–6940 (2017).
14. Lino, C. et al. Development of a QCM-based biosensor for the detection of non-small cell lung cancer biomarkers in liquid biopsies. *Talanta* **260**, 124624 (2023).
15. Lim, H. J., Saha, T., Tey, B. T., Tan, W. S. & Ooi, C. W. Quartz crystal microbalance-based biosensors as rapid diagnostic devices for infectious diseases. *Biosens. Bioelectron.* **168**, 112513 (2020).
16. Kim, J. H. et al. Technological advances in electrochemical biosensors for the detection of disease biomarkers. *Biomed. Eng. Lett.* **11**, 309–334 (2021).
17. Jing, L. et al. Electrochemical biosensors for the analysis of breast cancer biomarkers: from design to application. *Anal. Chem.* **94**, 269–296 (2022).
18. Wu, J., Liu, H., Chen, W., Ma, B. & Ju, H. Device integration of electrochemical biosensors. *Nat. Rev. Bioeng.* **1**, 346–360 (2023).
19. Joshi, A. et al. Recent advances in biosensing approaches for point-of-care breast cancer diagnostics: challenges and future prospects. *Nanoscale Adv.* **3**, 5542–5564 (2021).
20. Santos, M. S. F., Ameku, W. A., Gutz, I. G. R. & Paixão, T. R. L. C. Gold leaf: from gilding to the fabrication of disposable, wearable and low-cost electrodes. *Talanta* **179**, 507–511 (2018).
21. Prasertying, P. et al. Gold leaf electrochemical sensors: applications and nanostructure modification. *Analyst* **146**, 1579–1589 (2021).
22. Zamani, M. et al. Surface requirements for optimal biosensing with disposable gold electrodes. *ACS Meas. Au*. **2**, 91–95 (2022).
23. Zamani, M., Klapperich, C. M. & Furst, A. L. Recent advances in gold electrode fabrication for low-resource setting biosensing. *Lab. Chip*. **23**, 1410–1419 (2023).
24. Wongkaew, N., Simsek, M., Griesche, C. & Baeumner, A. J. Functional nanomaterials and nanostructures enhancing electrochemical biosensors and lab-on-a-chip performances: recent progress, applications, and future perspective. *Chem. Rev.* **119**, 120–194 (2019).
25. Mladenović, M. et al. Biosensors for cancer biomarkers based on mesoporous silica nanoparticles. *Biosensors* **14**, 326 (2024).
26. Vanova, V. et al. Peptide-based electrochemical biosensors utilized for protein detection. *Biosens. Bioelectron.* **180**, 113087 (2021).
27. Wang, X. et al. Applications of electrochemical biosensors based on functional antibody-modified screen-printed electrodes: a review. *Anal. Methods*. **14**, 7–16 (2021).
28. Villalonga, A., Pérez-Calabuig, A. M. & Villalonga, R. Electrochemical biosensors based on nucleic acid aptamers. *Anal. Bioanal Chem.* **412**, 55–72 (2020).
29. Patel, M., Agrawal, M. & Srivastava, A. Signal amplification strategies in electrochemical biosensors via antibody immobilization and nanomaterial-based transducers. *Mater. Adv.* **3**, 8864–8885 (2022).
30. Podunavac, I. et al. Low-cost goldleaf electrode as a platform for Escherichia coli immunodetection. *Talanta* **259**, 124557 (2023).
31. Kundacina, I. et al. Rapid and cost-effective fabrication of biosensors for salmonella detection. In *2023 IEEE Sensors* 1–4 https://doi.org/10.1109/SENSORS56945.2023.10325027 (IEEE, 2023).
32. Kittler, S., Besleaga, M., Ebner, J. & Spadiut, O. Protein l—more than just an affinity ligand. *Processes* **9**, 874 (2021).
33. Tran, T. et al. Process integrated biosensors for real-time monitoring of antibodies for automated affinity purification. *Anal. Methods*. **14**, 4555–4562 (2022).
34. Octet® Protein, L. (ed) (ProL) Biosensors. https://shop.sartorius.com/at/p/octet-protein-l-prol-biosensors/Bio-Layer-Interferometry-ProL-Biosensors.
35. Romih, T. et al. The effect of preconditioning strategies on the adsorption of model proteins onto screen-printed carbon electrodes. *Sensors* **22**, (2022).
36. Kittler, S. et al. Recombinant protein L: production, purification and characterization of a universal binding ligand. *J. Biotechnol.* **359**, 108–115 (2022).
37. Elgrishi, N. et al. A practical beginner's guide to cyclic voltammetry. *J. Chem. Educ.* **95**, 197–206 (2017).
38. Chowdhury, D. R., Spiccia, L., Amritphale, S. S., Paul, A. & Singh, A. A robust iron oxyhydroxide water oxidation catalyst operating under near neutral and alkaline conditions. *J. Mater. Chem. A*. **4**, 3655–3660 (2016).
39. Lazanas, A. C. & Prodromidis, M. I. Electrochemical impedance spectroscopy—A tutorial. *ACS Meas. Au*. **3**, 162–193 (2023).
40. Parkkila, P., Härkönen, K., Ilvonen, P., Laitinen, S. & Viitala, T. Protein A/G-based surface plasmon resonance biosensor for regenerable antibody-mediated capture and analysis of nanoparticles. *Colloid Surf. A*. **654**, 130015 (2022).
41. Harris, D. C. *Quantitative Chemical Analysis*. 1008 (W. H. Freeman, 2006).
42. Wignarajah, S., Chianella, I. & Tothill, I. E. Development of electrochemical immunosensors for HER-1 and HER-2 analysis in serum for breast cancer patients. *Biosensors* **13**, 355 (2023).
43. Wang, W., Han, R., Chen, M. & Luo, X. Antifouling peptide hydrogel based electrochemical biosensors for highly sensitive detection of cancer biomarker HER2 in human serum. *Anal. Chem.* **93**, 7355–7361 (2021).
44. Yang, X. et al. An electrochemical biosensor for HER2 detection in complex biological media based on two antifouling materials of designed recognizing peptide and PEG. *Anal. Chim. Acta*. **1252**, 341075 (2023).
45. Shamsipur, M., Emami, M., Farzin, L. & Saber, R. A sandwich-type electrochemical immunosensor based on in situ silver deposition for determination of serum level of HER2 in breast cancer patients. *Biosens. Bioelectron.* **103**, 54–61 (2018).
46. Wang, L. et al. An electrochemical biosensor to identify the phenotype of aggressive breast cancer cells. *Chem. Commun.* **59**, 3890–3893 (2023).
47. Zhang, Y. et al. A novel electrochemical biosensor based on AMNFs@ZIF-67 nano composite material for ultrasensitive detection of HER2. *Bioelectrochemistry* **150**, 108362 (2023).
48. Li, D., Zhang, W., Miao, M., Liu, Y. & Yang, H. A high-performance PEDOT:PSS platform electrochemical biosensor for the determination of HER2 based on carboxyl-functionalized MWCNTs and ARGET ATRP. *New. J. Chem.* **47**, 15579–15587 (2023).

Acknowledgements
This research was funded by the Europe Commission's Horizon 2020 Twinning program NANOFACTS (GA No. 952259), the Science Fund of the Republic of Serbia, (GA No. 7750276), Microfluidic lab-on-a-chip platform for fast detection of pathogenic bacteria using novel electrochemical aptamer-based biosensors – MicroLabAptaSens and Europe Commission's Horizon 2020 Teaming program ANTARES (GA No. 664387). IK, VR, and NK acknowledge the financial support of the. Ministry of Science, Technological Development, and Innovations of the Republic of Serbia (GA No. 451-03-66/2024-03/ 200358).

Author contributions
Ivana Kundacina: Conceptualization, Methodology, Investigation, Validation, Formal analysis, Visualization, Writing – original draft; Silvia Schobesberger: Conceptualization, Methodology, Validation, Formal analysis, Writing – review & editing; Stefan Kittler: Investigation, Formal analysis, Writing – review & editing; Helena Thumfart: Investigation, Formal analysis, Writing – review & editing; Oliver Spadiut: Writing – review & editing, Supervision; Peter Ertl: Writing - review & editing, Resources, Project administration; Nikola Ž. Knežević: Conceptualization, Writing – review & editing, Supervision, Project administration, Funding Acquisition; Vasa Radonic: Conceptualization, Methodology, Validation, Writing – review & editing, Supervision.

Declarations

Competing interests
The authors declare no competing interests.

Additional information
Supplementary Information The online version contains supplementary material available at https://doi.org/10.1038/s41598-024-83961-9.

Correspondence and requests for materials should be addressed to I.K. or V.R.

Reprints and permissions information is available at www.nature.com/reprints.

Publisher's note Springer Nature remains neutral with regard to jurisdictional claims in published maps and institutional affiliations.